Title: A STUDY ON ROOF POINT EXTRACTION BASED ON ROBUST ESTIMATION FROM AIRBORNE LIDAR DATA

Author's name: Shih-Hong Chio

Affiliation:

Address: Department of Land Economics, National Chengchi University

64, Chih-nan Rd., Sec. 2, Wenshan, Taipei 11623, Taiwan

E-mail: chio0119@nccu.edu.tw

TEL: +886-2-29393091 ext. 51657

FAX: +886-2-29390251

Abstract: The airborne LIDAR scanning system is a whole new surveying technique that captures extremely detailed and abundant terrain surface information. Terrain information is implied in airborne LIDAR data. Roof points are especially important in airborne LIDAR data for 3-D building reconstruction. The key point for automatically and reliably extracting roof points from airborne LIDAR data is how to exclude irrelevant non-roof points. Robust estimation is a theory about how to remove blunders from observations. If the non-roof points are viewed as blunders, it is possible to develop an algorithm to acquire the roof points, based on robust estimation theory. This paper will therefore study how to develop an algorithm to acquire those roof LIDAR points and remove irrelevant non-roof LIDAR points, based on robust estimation theory. Problems relevant to the proposed algorithm will be investigated in this study through experiments in order to understand the feasibility of the proposed algorithm and to further develop an automatic algorithm to extract roof points from airborne LIDAR data.

Key Words: LIDAR data, building reconstruction, robust estimation, quadtree split-and-merge.

Subject index: CI10 Survey Engineering

I. INTRODUCTION

The airborne LIDAR (short for **LI**ght **D**etection **A**nd **R**anging) scanning system is a whole new surveying technique that captures extremely detailed and abundant terrain surface information (Ackermann, 1999; Wehr and Lohr, 1999). Therefore a lot of terrain information is implied in airborne LIDAR data. Many algorithms

have been developed and proposed to extract important terrain information, such as the digital elevation model, the 3-D building model, and trees (Axelsson, 1999; Axelsson, 2000; Haala and Brenner, 1999; Maas and Vosselman, 1999; Priestnall *et al.*, 2000; Vosselman and Dijkman, 2001). For 3-D building models, roof points or planes in airborne LIDAR data should first be extracted. Most of the methods transform distributed LIDAR data into grid data through interpolation procedures and then apply image processing techniques to detect and extract them (Geibel and Stilla, 2000; Maas and Vosselman, 1999). Thus, some important spatial information, especially relating to height accuracies, may be lost (Axelsson, 2000). For this reason, some of these algorithms were developed using original airborne LIDAR data (Ackermann, 1999; Alharthy and Bethel, 2002; Elberink and Mass, 2000; Haala and Brenner, 1999; Priestnall *et al.*, 2000; Roggero, 2002; Schuster, 2004; Woo *et al.*, 2002; Vosselman and Dijkman, 2001). For example, Lee (2002) applies perceptual organization to analyze geometric structures of airborne LIDAR data in space and groups them into planes. Roggero (2002) proposes a region-growing-based segmentation that is feature based and is founded on principle component analysis of the static moments. Schuster (2004) presents an investigation on the use of Tensor Voting for categorizing LIDAR data into outliers, line elements (e.g. high-voltage power lines), surface patches (e.g. roofs), and volumetric elements (e.g. vegetation); that is, segmentation of LIDAR data using the tensor voting framework. Wang and Tseng (2004) present an octree-structure-based split-and-merge segmentation algorithm for organizing airborne LIDAR point cloud data into clusters of 3-D planes. Although the use of original airborne LIDAR data can keep the original accuracies, some difficulties still exist with roof point extraction from airborne LIDAR data. The challenging tasks are how to exclude the irrelevant points and how to extract roof points reliably and automatically. Additionally, no-one has yet developed an algorithm to extract roof points on the basis of blunder detection. In fact, the isolation of non-roof LIDAR points from coplanar roof LIDAR points can utilize the theory of blunder detection. In other words, non-roof LIDAR points can be viewed as blunders and removed during the extraction of roof points. Robust estimation is simply a theory about how to remove blunders from observations. Huber (1981) states that robustness signifies insensitivity to small deviations from the assumptions. Primarily, this is concerned with distributional robustness: the shape of the true underlying distribution deviates slightly from the assumed

model (usually the Gaussian law). The term "robust estimation" in this study means estimation techniques that are robust with respect to the presence of gross errors in the data. In this context, gross errors are defined as observations that do not fit the stochastic model of parameter estimation. Although the methods of Roggero (2002) and Schuster (2004) are robust, the meaning of "robust" in the methods of Roggero (2002) and Schuster (2004) is different from that in Huber (1981). This paper therefore presents a method of roof point extraction based on robust estimation and examines how to develop an algorithm for acquiring 3-D roof points from airborne LIDAR data from the perspective of blunder detection. For the first step, to roughly identify the locations and approximate area outlines of the roof(s) from pure airborne LIDAR data, aerial images with known orientation together with original LIDAR data are used to generate the orthoimages. Then, using a computer mouse device, the user depicts the approximate area outlines of the roof(s) on the orthoimages. Afterwards, on the assumption that roofs are composed of either horizontal or slope planes, some more accurate plane information, called GRID planes, is extracted from the LIDAR data that is extracted according to the approximate area outlines using least squares fitting, based on quadtree splitting (cf. Wang and Tseng, 2004). These GRID planes will be further merged using quadtree merging, according to the height constraints for providing SEED regions for merging the adjacent points, using the forward selection robust estimation approach (see Section II.3) to extract all the coplanar roof points. If only one roof exists, only one GRID plane is extracted. In this case, the SEED region is the GRID plane. Thus, the SEED region contains all the points in the approximate area outline. No matter how many roofs exist, the ground elevation is calculated and used to exclude non-roof SEED regions before they are used to merge adjacent points. In the proposed algorithm, it is essential for roof points to be reliably acquired; therefore, irrelevant points are considered as outliers and removed through robust estimation theory (Kubik *et al.*, 1986) to merge adjacent roof points. Section II will describe least squares fitting based on robust estimation theory for coplanar point extraction from airborne LIDAR data. The proposed algorithm will be presented in Section III. The experiments and results will be discussed and illustrated in Section IV. Finally, conclusions and suggestions for future research will be made in Section V.

II. COPLANAR POINT EXTRACTION THROUGH ROBUST ESTIMATION THEORY

This section explains how to extract coplanar points by least squares fitting based on robust estimation theory. Section II.1 describes how to extract coplanar points from sufficient airborne LIDAR points. The principle and use of robust estimation will be described in more detail in Sections II.2 and II.3, respectively.

1. Coplanar Point Extraction

In this study, on the assumption that building roofs are composed of either horizontal or oblique planes, any plane can be described by the following mathematical equation:

$$Z = aX + bY + c, \tag{1}$$

where *a, b,* and *c* are planar parameters; and *X, Y,* and *Z* are coordinate components.

Additionally, if the plane consists of *n* (>3) coplanar LIDAR points and only random errors occur in the *Z* coordinate component, the least squares adjustment of plane fitting can be expressed in matrix form as

$$\boldsymbol{L} + \boldsymbol{V} = \boldsymbol{AX} \ , \tag{2}$$

where $\boldsymbol{A} = \begin{bmatrix} X_1 & Y_1 & 1 \\ X_2 & Y_2 & 1 \\ \cdots & \cdots & \cdots \\ X_n & Y_n & Z_n \end{bmatrix}_{n*3}$ is the coefficient matrix, $\boldsymbol{X^T} = [a \quad b \quad c]_{1*3}$ is the estimated planar parameters vector, $\boldsymbol{L^T} = [Z_1 \quad Z_2 \quad \ldots \quad Z_n]_{1*n}$ is the observation matrix, and $\boldsymbol{V^T} = [v_1 \quad v_2 \quad \ldots \quad v_n]_{1*n}$ is the residual vector. If the weight of the observation is $\boldsymbol{P_{ll}} = \sigma_0^2 \boldsymbol{Q_{ll}}$, the estimation $\boldsymbol{X} = \boldsymbol{(A^T P_{ll} A)^{-1} (A^T P_{ll} L)}$ according to least squares principle. The sigma naught $\hat{\sigma}_0$ is equal to $\sqrt{\frac{\boldsymbol{V^T P_{ll} V}}{n-u}}$, where *u* is the number of unknowns, which can be used to verify the goodness of plane fitting.

2. Robust Estimation Theory (Klein and Foerstner, 1984)

The above-mentioned least squares fitting of coplanar LIDAR points is applicable to error-free data (i.e. blunder-free). Logically, erroneous observations cannot be treated with the same weights as error-free data, and have to be handled with reduced weights. All the observations must be introduced into the adjustment with weights chosen to correspond to their errors. The problem of locating gross errors is therefore synonymous with the determination of proper weights for the observations. An adjustment procedure that uses weight functions for complete elimination of the influence of gross errors is called the "method of robust estimation" (Kubik, 1984). After convergence of the iterative process, proper weights are determined for all observations and erroneous data will be given weights approximately equal to zero. This erroneous data will thus have no influence on the result of the adjustment. Many simple weight functions can be found that meet the conditions of robust estimators, but most of them cover only a small range of gross errors and will fail with the variety of gross errors occurring in practice. The reason for the failure in these cases is the assumption of linearity by the robust estimators (Huber, 1981). A lot of research has therefore been carried out to find a weight function and to develop a procedure that covers the wide range of gross errors (Werner, 1984). One renowned and effective weight function was developed by Klein and Foerstner (1984) and used in the block adjustment program PAT-M43. This weight function consists of the following hyperbolic function:

$$P = P_i \cdot F\left(v_i, \sigma_{v_i}, Q\right) = P_i \cdot \frac{1}{1 + (\alpha_i \mid v_i \mid)^d} \quad , \tag{3}$$

in which

$$\alpha_i = \frac{1}{1.4\hat{\sigma}_{v_i}} = \frac{\sqrt{P_i}}{1.4\hat{\sigma}_0\sqrt{r_i}} \tag{4}$$

$$d = 3.5 + \frac{82}{82 + Q^4} \tag{5}$$

$$Q = \frac{\hat{\sigma}_0}{\sigma_{a\ \ priori}} \tag{6}$$

$v_i =$ residual of observation i $\qquad$ $P_i =$ a priori weight observation i

$r_i =$ local redundancy of observation i $\qquad$ $\hat{\sigma}_{v_i} =$ estimated sigma of the residual v_i

$\hat{\sigma}_0 =$ estimated sigma-naught

By using the above-mentioned weight function, the robust estimator can be realized relatively easily while using a least squares algorithm and modifying the weights after each iteration step. Robust iteration steps are repeated until sufficient convergence is reached. The convergence is quite good, but highly correlated to the number and size of the gross errors as well as the geometric stability of the configuration. In this study, if the change of $\hat{\sigma}_0^2$ between two iteration steps becomes less than 0.001 after a corresponding iteration step, the final elimination of erroneous observations will be performed. All observations being used in that iteration step and getting $F\left(v_i, \sigma_{v_i}, Q\right) <$ *Threshold* will be marked as erroneous observations and will be given an infinitely small weight. The *Threshold* will be further discussed in the experimental data section. The other observations receive their original a priori weight. Some least squares iteration steps complete the procedure to reach the final result.

As mentioned above, robust estimation theory is embedded in an algorithm to isolate non-coplanar roof LIDAR points in this study. The detailed algorithm will be described in the next subsection. The following paragraph will explain how to calculate r_i in Eq. (4).

Based on Wolf and Ghilani (1997), the relation between the residual vector and the true error vector can be expressed in the following form:

$$\boldsymbol{V} = -\boldsymbol{Q}_{vv}\boldsymbol{P}_{ll}\boldsymbol{\varepsilon} \tag{7}$$

where $\boldsymbol{Q}_{vv} = \boldsymbol{P}_{ll}^{-1} - \boldsymbol{A}\boldsymbol{Q}_{xx}\boldsymbol{A}^T = \boldsymbol{Q}_{ll} - \boldsymbol{Q}_{\hat{l}\hat{l}}$ $\qquad$ $\boldsymbol{Q}_{xx} = (\boldsymbol{A}^T\boldsymbol{P}\boldsymbol{A})^{-1}$.

The *ith* diagonal element of $\boldsymbol{Q}_{vv}\boldsymbol{P}_{ll}$ is known as the local redundancy of observation *i*:

$$r_i = (\boldsymbol{Q}_{vv}\boldsymbol{P}_{ll})_{ii} \text{ and } r = \sum_{i=1}^{n} r_i \ . \tag{8}$$

$\hat{\sigma}_{v_i}$ can be also derived from $\boldsymbol{Q}_{vv}\boldsymbol{P}_{ll}$:

$$\hat{\sigma}_{v_i}^2 = (\boldsymbol{Q}_{vv})_{ii}\hat{\sigma}_0^2 = (\boldsymbol{Q}_{vv}\boldsymbol{P}_{ll}\boldsymbol{Q}_{ll})_{ii}\hat{\sigma}_0^2 = [\boldsymbol{Q}_{vv}\boldsymbol{P}_{ll}(\boldsymbol{Q}_{ll}\hat{\sigma}_0^2)]_{ii} \ . \tag{9}$$

If the observations are independent of each other, the matrices $\boldsymbol{Q}_{vv}$ and $\boldsymbol{P}_{ll}$ will be diagonal matrices.

Then

$$\hat{\sigma}_{v_i}^2 = (\boldsymbol{Q}_{vv}\boldsymbol{P}_{ll})_{ii}(\boldsymbol{Q}_{ll})_{ii}\hat{\sigma}_0^2 = (\boldsymbol{Q}_{vv}\boldsymbol{P}_{ll})_{ii}\sigma_{l_i}^2 \text{ or } \hat{\sigma}_{v_i} = \sqrt{r_i}\sigma_{l_i} \ . \tag{10}$$

3. Strategy for extracting all of the coplanar LIDAR roof points

The method to extract coplanar roof points from airborne LIDAR data and the theory to isolate non-coplanar roof points by robust estimation have been described in the previous two subsections. This subsection will further discuss the strategy for extracting all of the coplanar roof points through robust estimation theory. The proposed algorithm will be explained in more detail in the next section. Two approaches can be used for acquiring all the coplanar roof points. One is to include all coplanar roof points and irrelevant points in a dataset, and then robust estimation theory is implemented to remove the irrelevant points. The problem with this approach is how to ensure only one roof plane exists in the dataset. If many roof planes exist in the dataset, it is almost impossible to use robust estimation theory to completely extract the individual roofs. Conversely, if only part of all coplanar points on one roof is first acquired, it will be easier to merge relevant adjacent LIDAR points into a more complete roof by robust estimation theory. In other words, robust estimation theory can be implemented during the merging process to remove irrelevant LIDAR points. In this study, the idea of extracting the coplanar roof LIDAR points is known as forward selection strategy. The whole idea will be described in the next paragraph.

As mentioned in the previous paragraph, during the merging of adjacent roof LIDAR points, the part of all coplanar roof points on the same plane must first be extracted. This task is done by using a quadtree split-and-merge segmentation algorithm (cf. Wang and Tseng, 2004). First, quadtree splitting based on the least squares fitting principle is used to split the LIDAR data extracted according to the approximate area outlines (black dash outlines shown in Fig. 1 (a)) into GRID planes in which the sigma naught is less than one threshold (e.g. 0.12m), or the point number is less than one threshold, (e.g. 6). Fig. 1(b) shows the extracted GRID planes. Secondly, the GRID planes are merged as SEED regions in terms of height constraints (i.e. quadtree merging).

(a). Original LIDAR data

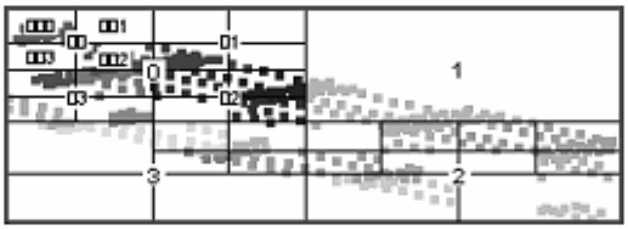

(b) Extracted GRID planes

(c) Extracted SEED regions

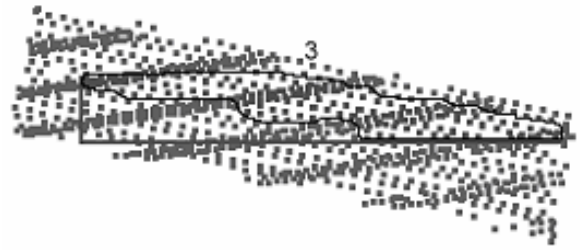

(d) Extracted ROOF points of one roof

Fig. 1 Illustration of the forward selection robust estimation approach

(different gray values for different heights in (a); different gray values for different planes in (b)~(d))

During the process of merging the GRID planes, the GRID plane with the most points is selected as the major GRID plane. The corresponding GRID centric heights can be calculated based on corresponding fitting plane parameters. Once a GRID plane adjacent to the major GRID plane is found, and if the difference between these two centric heights is less than one sigma naught of least squares fitting in the major GRID plane, this adjacent GRID plane is immediately merged into the major GRID plane. Then another adjacent GRID plane is searched again based on the proximity of the merged GRID plane and the major GRID plane. The same merging criterion is employed again. This process of merging GRID planes is continued until no more GRID planes can be merged. After the first SEED region is acquired, the second major GRID plane is selected again based on the point number. The merging process described above is carried out repeatedly to find the second SEED region. This process is carried on until no more SEED regions can be found. Figure 1(c) demonstrates the extracted SEED planes after merging the relevant GRID planes. If only one GRID plane is found within the area outlines, the SEED region will contains all the points in this outline.

After the SEED regions are acquired, the forward selection strategy of robust estimation is implemented to merge adjacent points for each SEED region. If the merged adjacent points are located in another SEED region, they will be removed from the corresponding SEED region. Moreover, adjacent points that have already been merged are not used in the extraction of other roof points. The adjacent points are determined by distance and geometric constraints, including height and normal direction. The distance constraint demands that the distance between adjacent points and at least two points in the SEED regions should be less than twice the average point distance. The height constraint requires that the difference between each point height and its calculated height, based on fitting planar parameters of the SEED region, should be within three times the reachable height accuracy of the airborne LIDAR surveying technique. Additionally, the normal direction derived from this point and the two points that are closest to this point in the SEED region should be similar to the normal direction of the SEED region. In other words, the difference between both normal directions should be less than one threshold (e.g. 15 degrees). Once the points in the SEED region and adjacent points are collected into a dataset, the robust estimation approach is used to exclude non-coplanar roof points and merge coplanar roof points into a new SEED region. Whenever one group of adjacent points is merged into

this new dataset, the new group of adjacent points is identified based on the same criterion. The forward selection robust estimation approach is then used again to merge the adjacent points. The same procedure is repeated until no adjacent points can be merged.

The three subsections above describe the relevant theory and strategy for merging adjacent coplanar roof LIDAR points. The following section will illustrate the proposed algorithm used in this study.

III. ALGORITHM FOR ROOF POINT EXTRACTION FROM AIRBORNE LIDAR DATA

This section will describe the proposed algorithm to extract coplanar roof points from airborne LIDAR data.

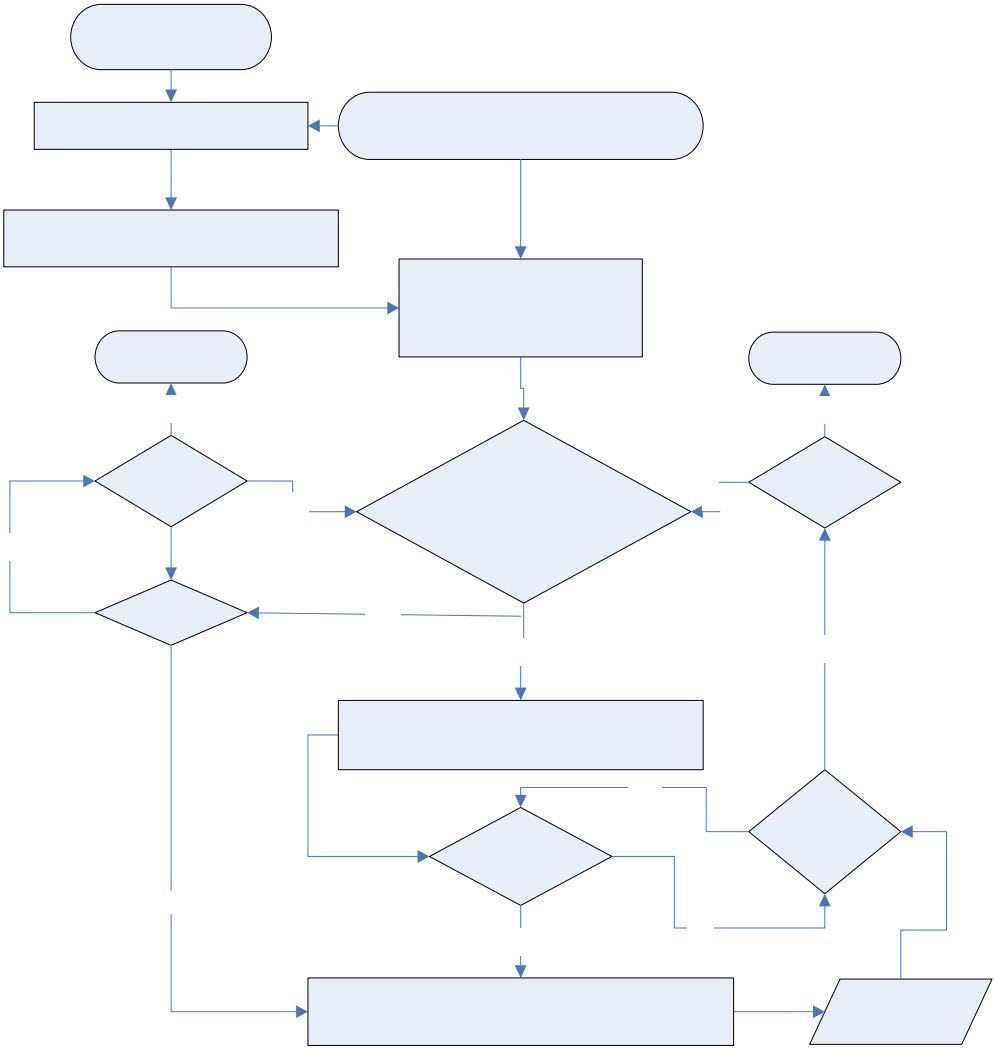

Fig. 2 Flowchart for this study

As the flowchart in Fig. 2 shows, the orthoimages are generated from original airborne LIDAR data and aerial images with known exterior parameters. The approximate area outlines covering the building roof(s) can then be roughly identified using a mouse device on a computer screen. The operators only identify the outlines; they do not need to locate them accurately. Several building roofs can be covered by one outline.

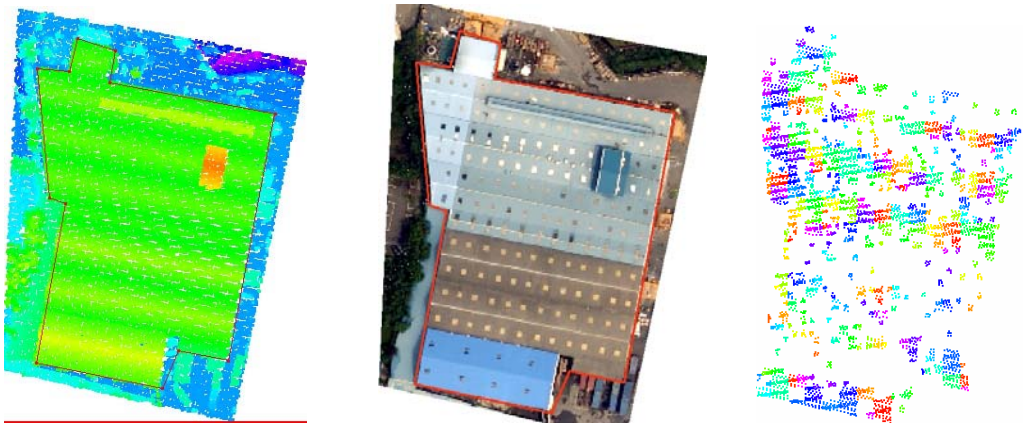

(a) Original LIDAR data (b) Orthoimage (c) Extracted GRID planes

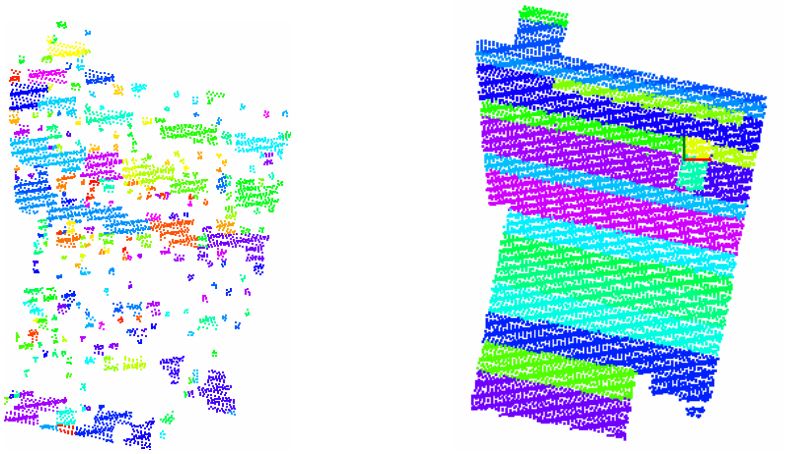

(d) Extracted SEED regions (e) Extracted roof planes

Fig. 3 Diagram of original dataset A, orthoimage, GRID planes, SEED regions, and extracted roofs

After each area outline covering the roof(s) is collected by the operator, the rectangular size covering each area outline is determined from the left-up and right-down outline points. As the area outlines are digitized roughly from orthoimages, it is necessary to extract LIDAR data from this rectangle range expanded 5 meters outward to ensure that all coplanar roof points are included for the forward selection robust estimation

approach. According to Section II.1, the σ_0 of plane least squares fitting of the LIDAR data in each area outline can be utilized for judgment of roof plane numbers when all the observations are viewed as having identical weights. If σ_0 is more than one threshold (e.g. 0.12m), more roofs might exist within this area outline. If it is not, only one roof plane exists. If more roof planes may exist, the quadtree spitting and merging algorithm is implemented, as shown in Fig. 1, to find the SEED regions for merging adjacent coplanar LIDAR points through robust estimation theory (see Section III.3). As shown in Fig. 3, SEED regions are constructed from original airborne LIDAR data (Fig. 3(a)) within the red outline, which is derived from the red outlines on the orthoimage (Fig. 3(b)) based on a quadtree split-and-merge segmentation algorithm. Fig. 3(c) shows extracted GRID planes and Fig. 3(d) extracted SEED regions.

No matter how many roof planes exist in the area outline, ground SEED regions should be excluded before the forward selection robust estimation approach is implemented to merge adjacent points. Ground SEED regions are excluded according to ground elevation. Ground elevation is calculated by averaging the height of the points that are located between 2% and 12% intervals after the points are sorted, based on their ascending height. If the difference between the average height of the SEED region and the ground elevation is less than one threshold (e.g. 3 meters), this SEED region is viewed as a non-roof SEED region. If only one roof plane exists in the area outline, all points in the SEED region are used to merge the adjacent points by the forward selection robust estimation approach. If more roofs might exist in the area outline, the SEED region with the most points is used to merge adjacent points by the forward selection robust estimation approach. The adjacent points are determined by distance and geometric constraints, as stated in Section II.3.

Whenever one group of adjacent points is merged, a new group of adjacent points is identified with a new dataset based on the same criterion. The forward selection robust estimation approach is used once more to merge adjacent points. The same procedure is repeated until no adjacent points can be merged. After all points on one roof are extracted, the other SEED region with the most points is found in the remaining SEED regions. The same procedure is continued until no SEED region and no area outline can be found for plane extraction. Fig. 3(e) shows all the extracted roofs according to the proposed algorithm from test dataset A.

Briefly, the proposed study procedure is subdivided into three steps: 1. Location of area outlines covering the roof(s) from orthoimages; 2. Determination of the possible roof numbers from LIDAR data in each outline based on the quadtree spit-and-merge algorithm; 3. Extraction of whole coplanar roof points by merging adjacent coplanar roof points based on the forward selection robust estimation approach. The experiments and the test results will be described in the next section.

IV. EXPERIMENTS

Three test datasets, as shown in Figs. 3 through 5, were extracted from airborne LIDAR data collected with Leica ALS50, in Hsinchu, Taiwan, in 2005. Each dataset covers buildings and other terrain objects. The airborne LIDAR data are purely surface data after filtering. Basic data characteristics are listed in Table 1. Figs. 3(a) through 5(a) illustrate the vertical views of the original LIDAR data. For ease of visualization, the heights are displayed in different colors and the point sizes are moderately enlarged. Figs. 3(b) through 5(b) illustrate the corresponding orthoimages, with 0.5m per pixel, generated from aerial images and the original LIDAR data using a Lecia Photogrammetry Suite. The red outlines overlaid on the orthoimages are collected roughly by the mouse device. The corresponding red outlines shown in Figs. 3(a) through 5(a) emphasize that the outlines collected from the orthoimages may not just include roofs. Some other terrain points are also contained in the collected outlines. The influences of the relevant thresholds on the result and problems concerning the proposed algorithm will first be investigated by testing dataset A in order to further develop an automatic algorithm to extract roof points from airborne LIDAR data. Secondly, the results for three datasets will be evaluated according to one set of thresholds, determined from the experimental results of dataset A, in order to understand the feasibility of the proposed algorithm.

Table 1 Description of three test datasets

Dataset	A	B	C
Numbers of outlines	1	6	4
Average point density (points/m^2) in each outline	(1).1.7	(1).1.7, (2).2.2, (3).1.9, (4).1.9, (5).1.9, (6).1.6	(1).2.3, (2).1.7, (3).1.9, (4).1.7
Description	Adjacent gable building roofs	Adjacent gable and flat building roofs with attached roof structures	Adjacent gable and flat building roofs with attached roof structures

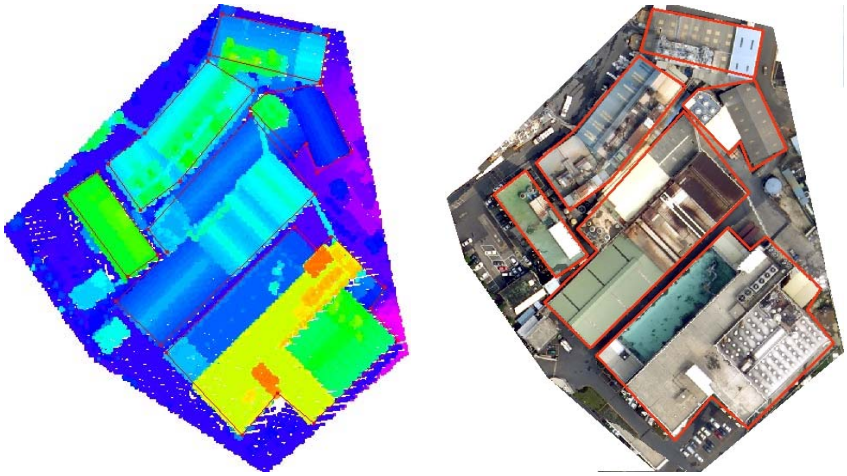

(a) Original LIDAR data (b) Orthoimage

Fig. 4 Original data and orthoimage for test dataset B

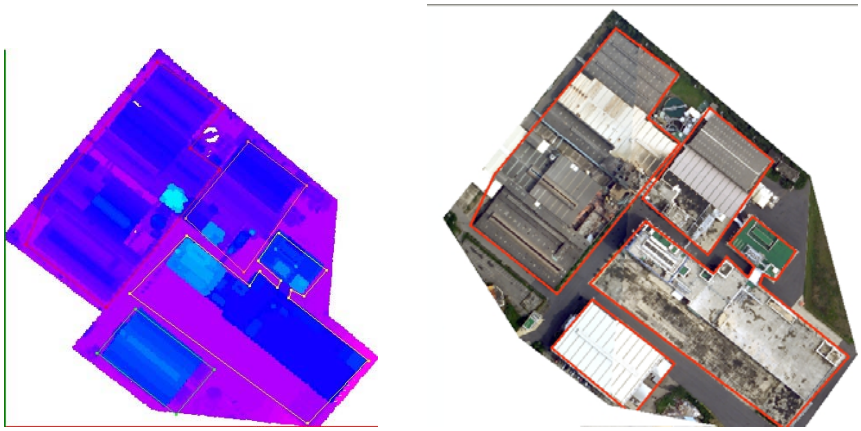

(a) Original LIDAR data (b) Orthoimage

Fig. 5 Original data and orthoimage for test dataset C

1. The influences of relevant thresholds on the result

This subsection investigates relevant thresholds that may affect the extraction results by using dataset A in order to get a better set of thresholds for automatic extraction of roof points The first important one is the threshold of the σ_0 for plane least squares fitting of the LIDAR data in each area outline for judgment of roof plane numbers. The threshold of the σ_0 also affects the number of GRID patches. The threshold of point numbers for plane least squares fitting in each GRID patch is also important, but it is fixed at 6 in this study. The subsequent three thresholds are concerned with the judgment of the proximity when using the forward selection robust estimation approach to merge the adjacent points. One threshold is the distance constraint of adjacent points, one is the height constraint, and the other is the normal direction constraint. Finally, the most important threshold for the results is the weight threshold for $F\left(v_i, \sigma_{v_i}, Q\right)$, including a priori σ. This threshold will be used to highlight the erroneous observations.

(i). *The weight thresholds for* $F\left(v_i, \sigma_{v_i}, Q\right)$

Since the most important threshold for the results is the weight threshold, this subsection will begin the investigation with this threshold. In order to understand how this threshold affects the extracted results, some thresholds must be fixed during the investigation. According to Leica Geosystems (2006), the reachable height accuracy of airborne LIDAR surveying is 0.15m. Therefore, the a priori σ in the weight threshold for $F\left(v_i, \sigma_{v_i}, Q\right)$ is fixed at 0.15m. Additionally, the threshold σ_0 of plane least squares fitting for judgment of the number of roof planes and for extracting the GRID patches is set at 0.12m, which is better than the reachable height accuracy of LIDAR surveying. It is also reasonable to set the height constraint as 3 times 0.15m, which is three times the reachable height accuracy of LIDAR surveying, for the judgment of proximity when merging adjacent points. In addition, the threshold for the distance constraint of adjacent points is set as twice the average point distance and the threshold for the normal direction constraint is not taken into account at this stage of the current test.

After fixing the above-mentioned thresholds, Table 2 shows the relationship between different weight thresholds for $F(v_i, \sigma_{v_i}, Q)$ and the extracted roof numbers. This experiment shows that the extracted roof number of 20 does not change if a weight threshold not greater than 1E-14 is adopted. In order to choose the best weight threshold for future tests, the number of extracted LIDAR points and the corresponding fitting σ for each roof in different weight thresholds, less than 1E-14, should be investigated in more detail.

Table 2: The relationship between the extracted roof numbers and different weight thresholds for $F(v_i, \sigma_{v_i}, Q)$

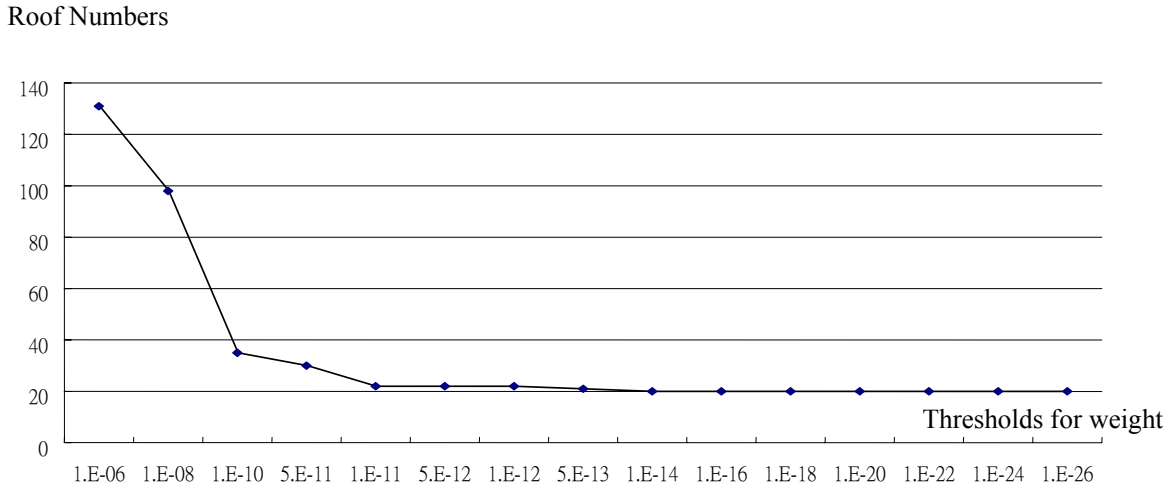

Table 3 gives the results of the weight thresholds that are not greater than 1E-14. It shows that the number of extracted LIDAR points and fitting σ for each roof does not change as the weight threshold decreases, when the thresholds are not greater than 1E-18. The chosen weight threshold for future tests is therefore 1E-18.

The a priori σ in (see also Eqs. (3) and (6)) should also be investigated to understand its influence on the results. Different values (e.g. 0.15m, 0.015m, 0.0015m, 0.1m, and 0.05m) are used for the tests. It was found that only the computing times were different; both the extracted roof numbers and the LIDAR points in each roof were the same. A smaller a priori σ needs much more time to extract the roof points but it does not change the results. The reachable height accuracy (i.e. 0.15m) of LIDAR surveying was therefore adopted as the a priori σ for the future tests.

After the determination of the weight threshold and the a priori σ in the weight threshold, the results for extracted roofs for dataset A are shown in Table 3 and Figure 6(a). The influences of the remaining thresholds on the results and the phenomena caused will be described in the next subsection.

Table 3: The extracted roof points with different weight thresholds and two different distance constraints

	2 times *sigma naught shown in ( ) when all observations have identical weight								1.75 times
	1.E-14	1.E-16	1.E-17	1.E-18	1.E-20	1.E-22	1.E-24	1.E-26	1.E-18
1	1580 (0.18)								1579(0.18)
2	1368(0.18)								1366(0.18)
3	961(0.13)								959(0.13)
4	305(0.17)								305(0.17)
5	1301(0.16)								1300(0.16)
6	**1316(0.14)**								**1295(0.14)**
7	**335(0.22)**	**416(0.25)**	**417(0.25)**	***639(0.28)***					***346(0.24)***
8	**870(0.13)**	**790(0.14)**	**789(0.14)**	***574(0.13)***					***863(0.13)***
9	817(0.13)								818(0.13)
10	***895(0.21)***								***896(0.21)***
11	1076(0.16)								1070(0.16)
12	**142(0.13)**	144(0.14)							144(0.14)
13	1009(0.15)								1010(0.15)
14	764(0.15)								761(0.15)
15	**111(0.13)**	**105(0.12)**	**105(0.12)**	93(0.12)					106(0.12)
16	595(0.14)								597(0.14)
17	**824(0.17)**	825(0.17)							827(0.17)
18	357(0.17)								357(0.17)
19	133(0.16)								132(0.16)
20	**100(0.14)**	98(0.14)							98(0.14)

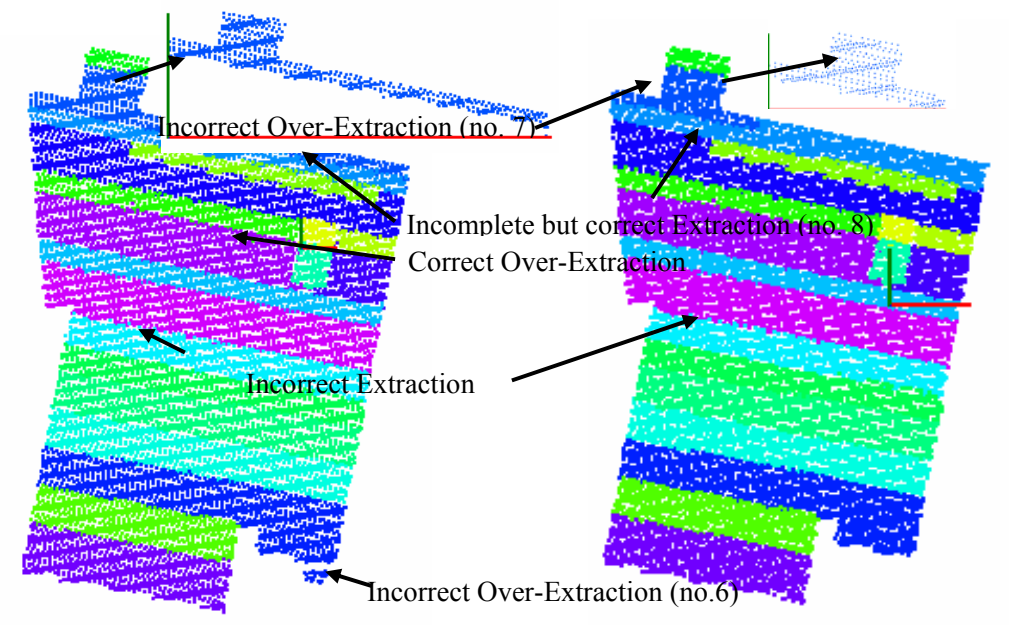

(a) 2 times average point distances (b) 1.75 times average point distances

Fig. 6 Extraction illustrations from dataset A with different distance constraints for adjacent points

(ii). *Some phenomena in the tests*

Some phenomena were found during the tests. The first phenomenon was that over-extraction occurred in two situations. One is the points with similar plane characteristics of extracted roof planes are close to the edge of extracted roof planes. The other one is the points without similar plane characteristics of extracted roof plane are close to the edge of extracted roof plane. In this case, this phenomenon will emerge due to the statistical properties of least squares fitting. Some over-extraction is correct when only some points near the roof are merged, as shown in Figs. 6 and 7. Some over-extraction is incorrect if these extracted roofs obviously cover other roofs or other terrain objects, as shown in Figs. 6 and 7. Clearly, some over-extraction is caused by a larger distance constraint. This could therefore be avoided by reducing the distance constraint; that is, 1.75 times instead of 2 times the average point distance. The obvious example is the extraction of roofs no. 6 and no. 7, as shown in Figs. 6 and 7 and Table 3. After reducing the distance constraints, the extraction of roof no. 6 is correct. Although the extraction of roof no. 7 is still incorrect, the point numbers with incorrect extraction are also reduced. However, it was also found that if the distance constraint is too small (e.g. 1 times

the average point distance), all the extracted roofs are incomplete. Conversely, over-extraction will be obvious. The threshold for the distance constraint of adjacent points was therefore fixed at 1.75 times the average point distance for subsequent tests.

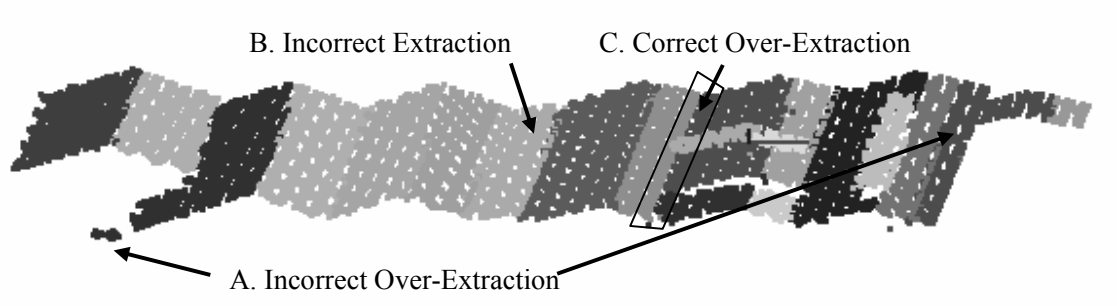

Fig. 7 Illustrations of over-extraction and incorrect extraction in dataset A

During the tests, it was also discovered that some incorrect extraction is caused by the characteristics of the roof plane, especially almost flat and elongated gable roofs. This case is shown in B in Fig. 7. This demonstrates that if the SEED region is located on an almost flat and elongated gable roof, all the points on this gable roof nearly pass the test of robust estimation. This will then lead to incorrect extraction. The sigma naught for this kind of plane extraction will usually be bigger, for example the sigma naught 0.21m of roof no. 10 in Table 3).

Since the location of the SEED region will cause incorrect extraction, is it possible to acquire a better SEED region by using smaller sigma thresholds for plane fitting so that this kind of incorrect extraction is avoided? Three different kinds of fitting to sigma thresholds were therefore studied. It was found that even when the threshold for the plane fitting sigma is fixed at 0.10m or 0.12m, roof no.10 is always acquired incorrectly, as shown in Figs. 8 (a), 8(b), and 9. The extraction of roof no. 7 will be correct if the threshold is set at 0.15m. We find that this is caused by the order of the extraction. This means that if roof no. 8 is extracted first, the extraction of roof no. 7 will be correct. This is illustrated in Fig. 9(c).

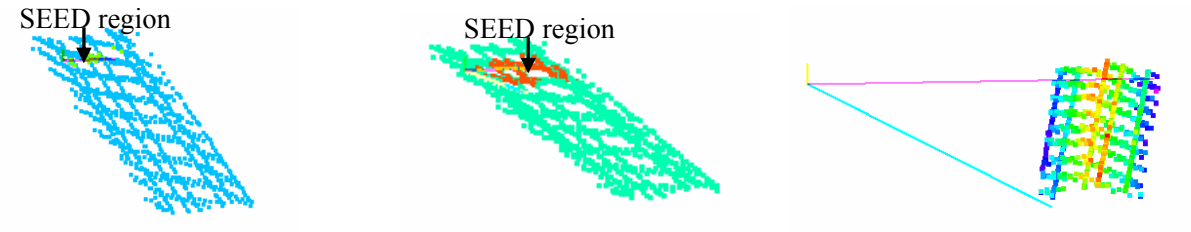

(a) 0.10m for fitting sigma threshold (b) 0.12m for fitting sigma threshold (c) Original data

Fig. 8 Illustration of incorrect extraction (no.10) caused by the locations of SEED regions and plane properties

Although the extraction of roof no. 7 is correct if the sigma threshold is set at 0.15m, a better result is acquired when the sigma threshold is 0.12m (from Table 4). Additionally, some over-extraction will be more obvious when the sigma threshold is 0.15m. Therefore, 0.12m will be used as the threshold of plane fitting sigma.

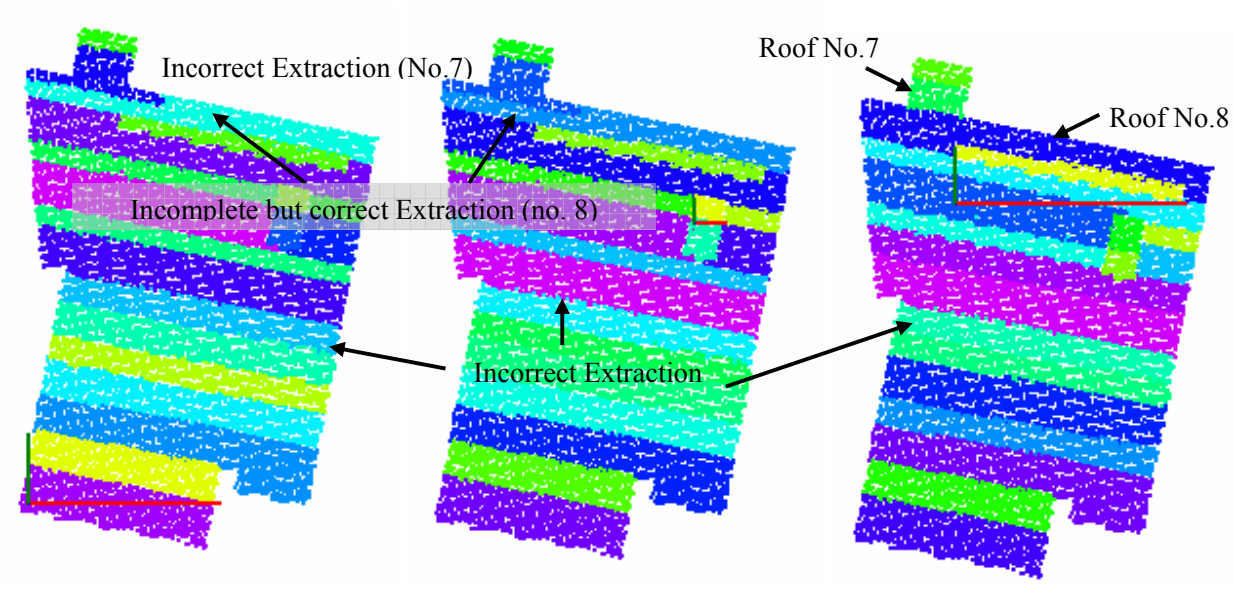

(a) (b) (c)

Fig. 9 The extracted results for different thresholds of plane fitting sigma: (a) 0.10m, (b) 0.12m, (c) 0.15m

Table 4 Extracted roofs and their corresponding sigma under different fitting threshold

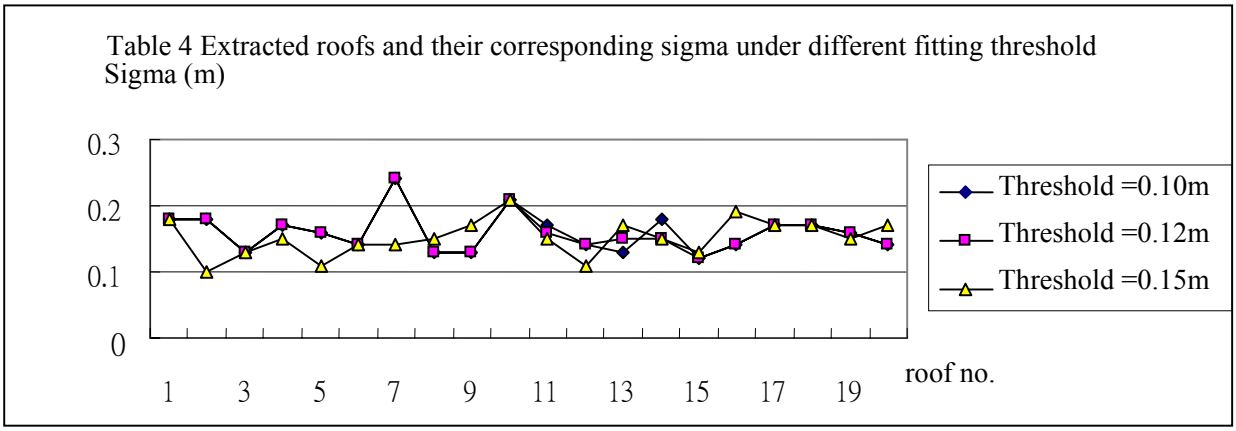

Having discussed incorrect over-extraction, let us now discuss correct over-extraction. It is the case that those extracted points are close to roof edges, as shown in Figs. 6 and 7. It is obvious that those are points with different normal directions with respect to the desirable extracted roof plane. Therefore, in the following test, different normal direction thresholds are respectively imposed on the proposed algorithm during the merging of adjacent points. Table 5 shows that the extracted roof numbers are more than 20 if the normal direction threshold is set too small and the roof numbers are maintained at 20 if the normal direction threshold is set at more than 15 degrees. Table 6 also shows that incorrect extraction in roof nos. 7 and 8 became correct extraction when the normal direction threshold was set at 16 degrees. Moreover, except for roof nos. 9, 10, 14, 18, and 20, all the sigma naughts increase as the threshold increases.

Table 5 Relationship between extracted roof numbers and normal direction thresholds

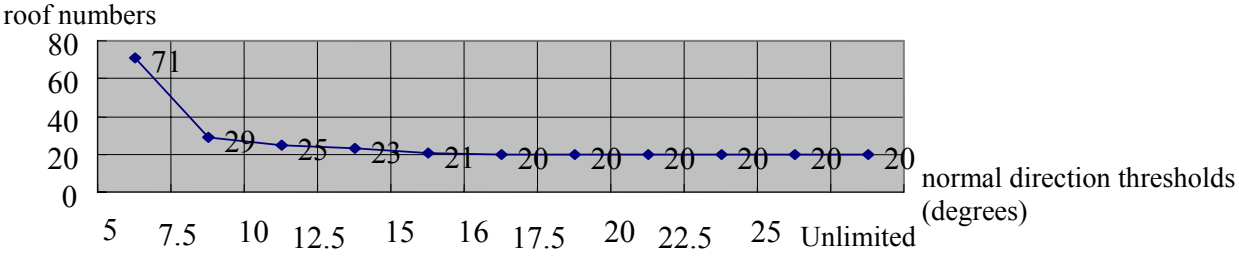

Table 6 Extracted points and corresponding sigma (meter) using different normal direction thresholds (degrees)						
	16	17.5	20	22.5	25	No limits
1	1397(0.130)	1421(0.136)	1472(0.149)	1513(0.160)	1525(0.162)	1579(0.176)
2	1247(0.144)	1283(0.153)	1305(0.159)	1309(0.160)	1330(0.166)	1366(0.177)
3	939(0.120)	941(0.121)	943(0.122)	949(0.125)	953(0.128)	959(0.131)
4	267(0.141)	275(0.147)	279(0.150)	281(0.152)	286(0.153)	305(0.171)
5	1179(0.118)	1191(0.121)	1221(0.131)	1241(0.138)	1260(0.143)	1300(0.159)
6	1263(0.130)	1269(0.131)	1279(0.134)	1285(0.135)	1290(0.138)	1295(0.139)
7	157(0.126)	***277(0.160)***	***285(0.171)***	***285(0.176)***	***300(0.193)***	***346(0.236)***
8	1035(0.136)	***920(0.133)***	***908(0.134)***	***910(0.134)***	***897(0.134)***	***863(0.134)***
9	**995(0.134)**	**958(0.134)**	**912(0.134)**	**882(0.133)**	**868(0.133)**	**818(0.133)**
10	***828(0.200)***	***858(0.207)***	***892(0.213)***	***902(0.214)***	***907(0.215)***	***896(0.213)***
11	1071(0.157)	1077(0.158)	1077(0.160)	1075(0.160)	1071(0.160)	1070(0.161)
12	137(0.119)	137(0.119)	140(0.130)	141(0.131)	141(0.131)	144(0.144)
13	997(0.142)	1001(0.143)	1000(0.143)	1011(0.149)	1011(0.149)	1010(0.149)
14	**129(0.135)**	**127(0.136)**	**125(0.135)**	**123(0.135)**	**120(0.134)**	**106(0.123)**
15	738(0.139)	720(0.139)	694(0.140)	678(0.140)	642(0.140)	597(0.139)
16	855(0.155)	842(0.155)	815(0.156)	789(0.156)	783(0.156)	761(0.154)
17	336(0.158)	339(0.160)	349(0.169)	354(0.172)	357(0.174)	357(0.174)
18	**149(0.154)**	**148(0.157)**	**147(0.156)**	**142(0.155)**	**142(0.155)**	**132(0.157)**
19	826(0.171)	830(0.172)	835(0.173)	832(0.173)	829(0.173)	827(0.173)
20	**103(0.144)**	**103(0.144)**	**101(0.143)**	**101(0.143)**	**101(0.143)**	**98(0.139)**

Comparing the results in Table 6 (the second column and last columns), it can be seen that when the normal direction threshold is set at 16 degrees, the extracted points in some roofs (e.g. roof nos. 1-6) are less than the extracted points without a normal direction threshold. This demonstrates that the phenomenon of over-extraction will be improved by the constraint of normal direction during the merging of adjacent points. However, this phenomenon cannot be avoided completely by the constraint of normal direction due to the statistical properties of least squares, unless the other data source can be fused into the proposed algorithm; for example, roof boundaries from building plan maps or aerial images. In any case, the imposed normal direction threshold can improve some over-extraction problems. In the following tests, 16 degrees will therefore be used as the threshold of normal direction constraints.

2. The completeness of extraction

The previous subsection investigated the relevant thresholds and phenomena for the extracted results. This subsection will use the relevant threshold setup from the previous subsection to further discuss the extracted statistics for the proposed algorithm.

The extracted results of the proposed algorithm from these datasets and collected area outlines are shown in Figs. 10(a), (b), and (c). Table 7 gives the statistics for the extracted results of these three test datasets. Apart from dataset A, there are many small attached rooftop structures on the major roofs in datasets B and C. It is difficult to identify whether some small structures are roof structures from the aerial images or orthoimages. However, the statistics for datasets B and C are presented as completely as possible in Table 7.

Most complex and small attached rooftop structures on the roofs in datasets C and D lead to incorrect or incomplete roof extraction. Some of the attached roof points cannot be extracted because they are too small and have fewer LIDAR points on them. Some of them cannot be extracted because they are not planar roofs. In addition, the threshold of 3m is set to exclude ground SEED regions for plane growing in this study. Non-roof points are therefore completely excluded in these three datasets. In dataset C, lots of small or thin strips belonging to the attached rooftop structures were extracted because the point numbers for roof SEED regions should be more than 6 points. Overall, from Table 7 and Figs. 10(a), (b), and (c), the average correct extracted rate is about 86% and the average percentage of completeness is also about 86%. Most of the points on the major roof structures are extracted; incorrect and incomplete roof extraction belong to the complicated and small attached building structures.

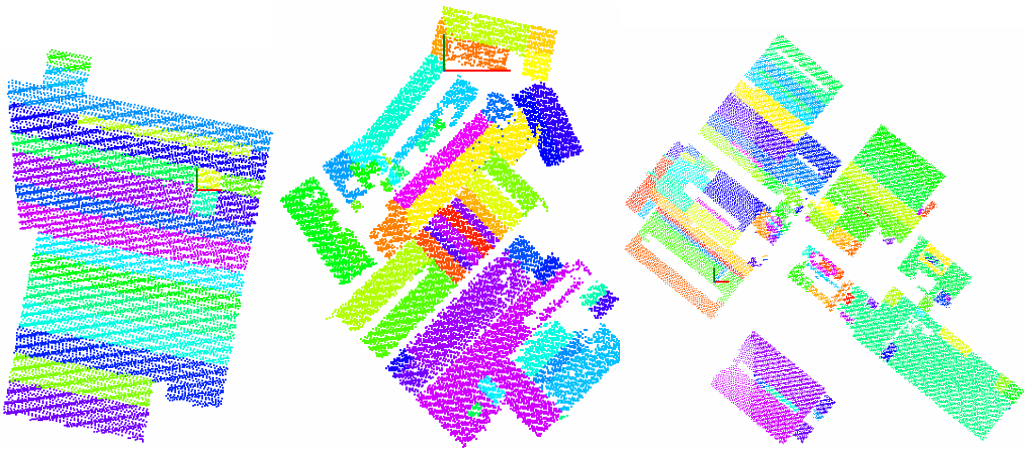

(a) Result for dataset A (b) Result for dataset B (c) Result for dataset C

Fig. 10 Extracted results for the three test datasets

Table 7 Extracted statistics for the three test datasets

Dataset	A	B	C
(A). Total roof planes	21	60	83
(B). Total extracted roof planes	20	49	111
(C). Correct roof extraction	19	45	78
(D). Correct but incomplete roof extraction	0	1	27
(E). Incorrect roof extraction	1	3	6
(F). Omission roof extraction	0	10	4
Correct extraction rates (C/B*100%)	95%	92%	70%
Completeness (C/A*100%)	90%	75%	94%

V. CONCLUSIONS AND SUGGESTIONS FOR FUTURE RESEARCH

The airborne LIDAR scanning system is a whole new surveying technique that captures extremely detailed and abundant terrain surface information. Terrain information is implied in airborne LIDAR data. The roof points in airborne LIDAR data are especially important for 3-D building reconstruction. The extraction of

building roof points from airborne LIDAR data is therefore an important task for 3-D building reconstruction. The most difficult part of roof point extraction from airborne LIDAR data lies in how to exclude the irrelevant data and how to extract the required data both reliably and completely. This paper proposed an algorithm to acquire roof LIDAR points and remove irrelevant non-roof LIDAR points based on robust estimation theory. From the experiments, the relevant problems concerning the proposed algorithm have been investigated and one set of thresholds has been used to extract roof points from airborne LIDAR data automatically. Both the average correct extracted rate and the average percentage of completeness are about 86% in the proposed algorithm. In addition, almost all of the major roof structures were extracted by the proposed algorithm in the three test datasets. The experiments have proved the feasibility of the proposed algorithm, and the possibility of automatically extracting roof points from airborne LIDAR data has also been raised. The proposed methodology does remove the relevant data from desirable roof planes from the experiments. However, the approximate outlines covering roofs were collected manually in this study. Future work could therefore acquire these area outlines automatically from another data source or from LIDAR data itself using image processing techniques. These experimental results also show that other data should be integrated for a more accurate extraction of roof points. Subsequent studies should therefore be conducted by integrating different data sources (e.g. aerial images), based on current results, for a much more complete reconstruction of building models.

ACKNOWLEDGEMENT

The author would like to acknowledge three anonymous referees for thoughtful comments and suggestions. However, the author will be responsible for any omissions or errors about this paper. Also, the author would like to thank Ministry of the Interior, Taiwan, R.O.C. for providing the test LIDAR datasets.

NONMENCLATURE

$\boldsymbol{A}$ the coefficient matrix

$F(v_i, \sigma_{v_i}, Q)$ the correct factor for the weight of observation *i*

$\boldsymbol{L}$ the observation matrix

n the number of observations

P the weight function of the observations

P_i a priori weight of the observation *i*

$\boldsymbol{P}_{ll}$ the weight matrix of the observations

$\boldsymbol{Q}_{ll}$ the co-factor matrix of observations

$\boldsymbol{Q}_{\hat{l}\hat{l}}$ the co-factor matrix of observations after adjustment

$\boldsymbol{Q}_{vv}$ the co-factor matrix of residuals

r_i the local redundancy of observation *i*

$\boldsymbol{X}$ the estimated parameters vector

u the number of unknowns

$\boldsymbol{V}$ the residual vector

v_i the residual of observation *i* , meter in SI unit.

$Z = aX + bY + c$ planar equation, where *a, b,* and *c* are planar parameters; and *X, Y,* and *Z* are coordinate components, meter in SI unit.

σ_0 the priori sigma-naught, meters in SI unit.

$\hat{\sigma}_0$ the estimated sigma-naught, meter in SI unit.

$\sigma_{a\ priori}$ the priori sigma-naught, meter in SI unit.

$\hat{\sigma}_{v_i}$ the estimated sigma of the residual v_i, meter in SI unit.

REFERENCES

1. Ackermann, F., 1999, "Airborne Laser Scanning - Present Status and Future Expectations," *ISPRS Journal of Photogrammetry & Remote Sensing*, Vol. 54, No. 2, pp. 64-67.

2. Alharthy, A., and Bethel, J., 2002, "Heuristic Filtering and 3D Feature Extraction from LIDAR data," *International Archives of Photogrammetry and Remote Sensing*, Vol. 33, Part A, pp. 29-34.

3. Axelsson, P., 1999, "Processing of Laser Scanner Data - Algorithms and Applications," *ISPRS Journal of Photogrammetry & Remote Sensing*, Vol. 54, No. 2, pp. 138-147.

4. Axelsson, P., 2000, "DEM Generation from Laser Scanner Data Using Adaptive TIN Models," *International Archives of Photogrammetry and Remote Sensing*, Vol. 33, Part B4/1, pp.110-117.

5. Elberink, S. O., and Maas, H., 2000, "The Use of Anisotropic Height Texture Measure for The Segmentation of Airborne Laser Scanner Data," *International Archives of Photogrammetry and Remote Sensing*, Vol. 33, part B3/2, pp. 678-684.

6. Geibel, R. and Stilla, U., 2000, "Segmentation of Laser Altimeter Data for Building Reconstruction: Different Procedures and Comparison," *International Archives of Photogrammetry and Remote Sensing*, Vol. 33, Part B3, pp.326-334.

7. Huber, P.J., 1981, *Robust Statistics*, John Wiley & Sons, Inc., p.1, New York, USA.

8. Haala, N. and Brenner, C., 1999, "Extraction of Building and Trees in Urban Environments," *ISPRS Journal of Photogrammetry & Remote Sensing,* Vol. 54, No. 2, pp. 130-137.

9. Klein, H., and Foerstner, W., 1984, "Realization of Automatic Error Detection in the Block Adjustment Program PAT-M43 Using Robust Estimators," *International Archives of Photogrammetry and Remote Sensing*, Vol.25, Part 3A, pp. 234-245.

10. Kubik, K., D. Merchant, and T. Schenk, 1986, "Grosserrors and robust estimation," *Technical Papers,* 1986 ACSM-ASPRS Annual Convention, Vol. 4, pp.250-255, Washington D.C.

11. Lee, I., 2002, "Perceptual Organization of Surfaces," *PhD. Dissertation*, Graduate Program in Geodetic Science and Surveying, The Ohio State University, Columbus, OH, USA.

12. Leica Geosystems, 2006, ALS50 Airborne Laser Scanner Introduction, Available :http://gis.leica-geosystems.com/, Leica Geosystems, Georgia, USA (last date accessed 1, March, 2006).

13. Maas, H. G. and Vosselman, G., 1999, "Two Algorithms for Extracting Building Models from Raw Laser Altimetry Data," *ISPRS Journal of Photogrammetry & Remote Sensing*, Vol. 54, No. 2, pp. 153-163.

14. Priestnall, G., Jaafar, J., and Duncan, A., 2000, “Extracting Urban Feature from LiDAR Digital Surface Models,” *Computers, Environment and Urban Systems*, Vol. 24, No. 2, pp. 65-78.

15. Roggero, M., 2002, “Object segmentation with region growing and principal component analysis,” *International Archives of Photogrammetry, Remote Sensing and Spatial Information Sciences,* Vol. 34 Part 3A, pp. 289–294.

16. Schuster, H.F., 2004, “Segmentation of Lidar Data Using The Tensor Voting Framework,” *International Archives of Photogrammetry, Remote Sensing and Spatial Information Sciences,* Vol. 35, Part B3, pp. 1073–1078.

17. Wang, M. and Tseng, Y-H., 2004, “LIDAR data segmentation and classification based on octree structure,” *International Archives of Photogrammetry, Remote Sensing and Spatial Information Sciences,* Vol. 35, Part B3, pp. 1682-1750.

18. Wehr, A. and Lohr, U., 1999, “Airborne Laser Scanning-An Introduction and Overview,” *ISPRS Journal of Photogrammetry & Remote Sensing*, Vol 54, No. 2, pp.68-92.

19. Werner, H. 1984, “Automatic Gross Error Detection by Robust Estimators,” *International Archives of Photogrammetry and Remote Sensing*, Vol. 25, Part 3, pp.197-219.

20. Wolf, Paul R. and Ghilani, Charles D., 1997, *Adjustment Computations: Statistics and Least Squares in Surveying and GIS.* John Wiley & Sons, Inc., pp.402-406, NY, USA.

21. Woo, H., Kang, E., Wang, S., and Lee, K. H., 2002, “A New Segmentation Method for Point Cloud Data,” *International Journal of Machine Tools & Manufacture*, Vol. 42, No. 2, pp. 167-178.

22. Vosselman, G. and Dijkman, S., 2001, “3D Building Model Reconstruction from Point Clouds and Ground Plans,” *International Archives of Photogrammetry and Remote Sensing*, Vol. 34, Part 3/W4, pp.37- 44.